⌘ *Author's Choice*

Calcium-induced Mechanical Change in the Neck Domain Alters the Activity of Plant Myosin XI*⑤

Motoki Tominaga[‡1], **Hiroaki Kojima**[‡], **Etsuo Yokota**[§], **Rinna Nakamori**[‡], **Michael Anson**[¶], **Teruo Shimmen**[§], and **Kazuhiro Oiwa**[‡§2]

From the [‡]*Advanced ICT Research Institute, National Institute of Information and Communications Technology, Kobe 651-2492, Japan,* the [§]*Department of Life Science, Graduate School of Life Science, University of Hyogo, Harima Science Park City, Hyogo 678-1297, Japan,* and the [¶]*Division of Physical Biochemistry, National Institute for Medical Research, The Ridgeway, Mill Hill, London NW7 1AA, United Kingdom*

Background: Cytoplasmic streaming driven by myosin XI is inhibited by Ca^{2+} in plant cells.
Results: The neck length and step size of a single myosin XI molecule decreased through Ca^{2+}-induced calmodulin dissociation.
Conclusion: Plant myosin XI is regulated by Ca^{2+} through dissociation of calmodulin, a different manner of regulation than for vertebrate myosin V.
Significance: Ca^{2+} affects the mechanical properties of myosin XI.

Plant myosin XI functions as a motor that generates cytoplasmic streaming in plant cells. Although cytoplasmic streaming is known to be regulated by intracellular Ca^{2+} concentration, the molecular mechanism underlying this control is not fully understood. Here, we investigated the mechanism of regulation of myosin XI by Ca^{2+} at the molecular level. Actin filaments were easily detached from myosin XI in an *in vitro* motility assay at high Ca^{2+} concentration (pCa 4) concomitant with the detachment of calmodulin light chains from the neck domains. Electron microscopic observations showed that myosin XI at pCa 4 shortened the neck domain by 30%. Single-molecule analysis revealed that the step size of myosin XI at pCa 4 was shortened to 27 nm under low load and to 22 nm under high load compared with 35 nm independent of the load for intact myosin XI. These results indicate that modulation of the mechanical properties of the neck domain is a key factor for achieving the Ca^{2+}-induced regulation of cytoplasmic streaming.

Cytoplasmic streaming, the high-velocity transport of organelles along actin cables, occurs in plant cells ranging from algae to angiosperms. At velocities of up to 60 μm s^{-1}, such streaming is the fastest known actin-myosin movement (1–3). Myosin XI plays an important functional role within plant cells in driving actin-based motility, including cytoplasmic streaming (4). Although Ca^{2+} is reported to have an inhibitory effect on cytoplasmic streaming in plant cells such as pollen tubes of lily (*Lilium longiflorum*) (5), stamen hair cells of *Tradescantia* (6),

trichome cells of tomato (7), and leaf cells of *Vallisneria gigantea* (8), the molecular mechanisms underling this regulation are not well understood. Difficulties in expressing and purifying large quantities of plant myosins have hampered progress in biochemical studies on plant myosins and their regulation. Recently, a single-molecule assay paved the way to overcome these problems (9).

Higher plant myosin XI has a molecular morphology similar to that of myosin V. Myosin XI has two head domains including elongated necks ~33 nm long, with each having six IQ motifs per heavy chain as light chain-binding domains followed by an α-helical coiled-coil region that couples two monomers (9). Higher plant 175-kDa myosin XI purified from cultured tobacco BY-2 cells has calmodulin (CaM)[3] as light chains (10) and moves processively on actin filaments toward its plus-end in 35-nm steps at 7 μm s^{-1}, the highest velocity thus far observed for a processive motor (9).

Mechanical processivity is an index for estimating the number of mechanochemical cycles carried out by a motor molecule per diffusional encounter with its polymer track. The high processivity of myosin XI is thought to adapt myosin for its role in organelle transport because each myosin molecule travels for a long distance (>1 μm) before dissociating from the actin track (9). Thus, only a small number of molecules need to be attached to each organelle to carry it many micrometers along actin cables *in vivo*. Studies on myosin Va led to the proposal of a putative hand-over-hand model based on a lever arm theory for such processive movement (11–13). A small change in the catalytic motor domain induced by ATP hydrolysis is amplified to a large displacement through a relatively rigid neck domain; this mechanical change corresponds to the power stroke. The neck domain is composed of six IQ domains with six bound light chains (all or mainly CaMs) and serves as a lever arm that enables myosin Va molecules to move as if they were walking on pseudorepeats of actin filaments 35 nm apart. According to this

---

⌘ *Author's Choice*—Final version full access.

⑤ This article contains supplemental Figs. 1 and 2.

[1] Present address: Molecular Membrane Biology Laboratory, RIKEN Advanced Science Institute, Wako, Saitama 351-0198, Japan.

[2] To whom correspondence should be addressed: Advanced ICT Research Institute, National Institute of Information and Communications Technology, Kobe 651-2492, Japan. Tel.: 81-78-969-2110; Fax: 81-78-969-2119; E-mail: oiwa@nict.go.jp.

---

[3] The abbreviations used are: CaM, calmodulin; pN, piconewtons.

model, the long neck domain with two heads is indispensable for processive movement.

The *in vivo* functions of various types of myosins are controlled both temporally and spatially. This control is partly accomplished by the regulation of myosin activity at the molecular level. In the case of myosin Va, the binding of Ca^{2+} to neck-associated light chains (CaMs) causes their dissociation and modulates the processive movement (14, 15). Thus, the modulation of the processivity is a possible common mechanism of regulation. Here, we investigated the Ca^{2+} sensitivity of the structural and functional properties of 175-kDa myosin XI isolated from tobacco (*Nicotiana tabacum*) BY-2 cells and show that its processive movement is regulated via the dissociation of CaM, which is a different manner of regulation than for vertebrate myosin Va. These results suggest that the regulation of the processivity through Ca^{2+}-induced CaM dissociation is variable and adjusted to the intracellular function of each myosin.

EXPERIMENTAL PROCEDURES

Protein Preparation—Myosin XI (175 kDa) was isolated from cultured tobacco (*N. tabacum*) BY-2 cells from 5-day-old cultures through co-sedimentation with rabbit skeletal muscle F-actin and an anion exchange column as described previously (9, 10).

Kinetic Experiments—Steady-state actin-activated ATPase was measured with an enzyme-coupled assay (E-6646, Molecular Probes, Eugene, OR) at 20 °C in assay buffer containing 25 mM KCl, 4 mM $MgCl_2$, 1 mM EGTA, 1 mM DTT, and 25 mM HEPES-KOH (pH 7.5) with or without $CaCl_2$ and various concentrations of rabbit skeletal F-actin as described previously (9). The desired concentrations of free Ca^{2+} were calculated with MAXCHELATOR and obtained by adding the specified amounts of $CaCl_2$ to the solution.

Electron Microscopy—Negatively stained myosin XI was prepared as described previously (16). Freshly prepared myosin XI in buffer (25 mM MOPS, 1 mM EGTA, 4 mM $MgCl_2$, and 10 mM ATP) with or without $CaCl_2$ was applied to carbon grids that were pretreated in a plasma cleaner for 3 s to make the carbon grid surface hydrophilic. After washing the grid with the same buffer without ATP, myosins were stained with 1% uranyl acetate. Micrographs were taken at ×40,000 magnification.

Immunoprecipitation—CaM dissociation from myosin XI exposed to Ca^{2+}-containing solutions was examined by immunoblotting with immunoprecipitation. 175-kDa myosin XI was associated with protein A-conjugated Sepharose beads (GE Healthcare) that were preincubated with antibody against the C-terminal peptide of 175-kDa myosin XI (17). The myosin-bound beads were washed six times with assay buffer with or without Ca^{2+}. The proteins bound to the beads were subjected to SDS-PAGE and analyzed by immunoblotting using antibody against the 175-kDa heavy chain (18) or CaM (19).

In Vitro Motility Assays, Single-molecule Assays, and Optical Trap Nanometry—*In vitro* motility assays were performed in a 10-μl flow chamber made from two nitrocellulose-coated coverslips (24 × 40 and 18 × 18 mm) with two slivers of polycarbonate film for spacing as described previously (9). Tetramethylrhodamine-labeled actin filaments were introduced onto the myosin-fixed surface in assay buffer with various concentrations of ATP and Ca^{2+} at 20 °C. Wild-type CaMs from bovine testes were purchased from Sigma (P1413). Before perfusing EGTA or Ca^{2+} solution into the flow chamber, the number of actin filaments that were bound and moving on the myosin surface was counted. After perfusing the solutions to be examined, the number of moving actin filaments was counted and shown as a percentage against the number of actin filaments before perfusion. The number of actin filaments that moved continuously over 5 μm was calculated to obtain the mean for three independent observation fields.

Optical trap nanometry was performed as described previously (9) with some modifications. Protein G-coated polystyrene carboxylated beads 200 nm in diameter were incubated with anti-C-terminal peptide antibody. After washing, the coated beads were added to myosin XI solutions. After washing with assay buffer with or without Ca^{2+}, myosin-bound beads were applied to actin filaments fixed onto a coverslip via an avidin-biotin interaction. The experiments were performed with a mixing ratio of 1:30 beads/myosin or less, where the probability of occurrence of bead movement was <40%. Consideration of this probability together with the geometry of myosin molecules on a bead indicated that >95% of movement observed was by a single myosin molecule. The displacement of the bead was measured using a quadrant photodiode system under dark-field illumination (20). Linearity of the trapped bead displacements detected by quadrant photodiode was verified up to ±300 nm by applying a sinusoidal displacement with various offsets to the trap position and recording the output signal (20). The steps were detected as a rapid positional change (within one to two sample points) followed by a dwell (>10 sample points) from the 100-Hz low pass-filtered trace. The step size was estimated from the difference between the mean pre-step and post-step positions. Trap stiffness was 0.0038 piconewtons (pN) nm^{-1}, which was determined from the variance of the Brownian fluctuation of the beads.

RESULTS

Effect of Ca^{2+} on Myosin XI Motility—The effects of Ca^{2+} on the motility of myosin XI were examined using a conventional *in vitro* motility assay in which rhodamine-phalloidin-labeled actin filaments glide over glass surfaces coated with myosin XI (10, 21). Fig. 1 shows the numbers of actin filaments bound and those moving on a myosin-coated surface in the presence of ATP after perfusing assay buffer containing EGTA or various concentrations of free Ca^{2+}. The number of moving actin filaments decreased as the Ca^{2+} concentration increased (Fig. 1A). At *p*Ca 4, all moving actin filaments readily dissociated from the surface, even with a moderate perfusion. This observation suggests that the affinity between an actin filament and myosin XI and/or the fraction of time that the myosin binds tightly to an actin filament during its ATPase cycle decreases at high concentrations of Ca^{2+} (*p*Ca <5.5). The percentage of the nonmotile actin filaments tightly bound to the surface compared with the moving actin filaments pre-perfusion did not change in EGTA or at various concentrations of Ca^{2+}, suggesting that they were tightly bound on the surface via nonspecific interactions (Fig. 1A).
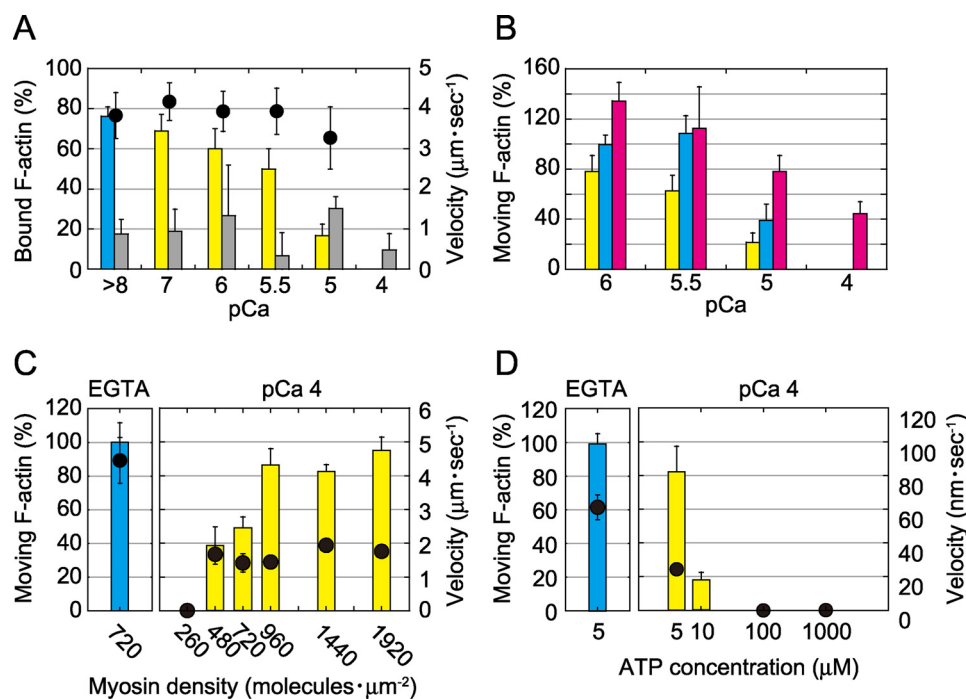
FIGURE 1. **Effect of Ca^{2+} in an *in vitro* motility assay of myosin XI.** *A*, effects of Ca^{2+} on the number of actin filaments. Shown is the percentage of moving actin filaments in EGTA (*blue bars*) and Ca^{2+} (*yellow bars*) and of non-moving (*gray bars*) actin filaments after the perfusion of solutions containing EGTA or various concentrations of Ca^{2+}. The number of actin filaments in EGTA that were bound and those moving on the surface before the perfusion of solutions was set at 100%. The velocity of moving actin filaments is shown (*black circles*). *B*, recovery of actin movement after treatment with Ca^{2+}. Perfusion with Ca^{2+} reduced the number of actin filaments on the myosin surface (*yellow bars*). Next, 1 mM EGTA and 24 nM actin filaments were perfused (*blue bars*). Then, both 24 nM actin filaments and 10 μM CaMs were perfused in 1 mM EGTA buffer (*red bars*). All experiments were performed in the presence of 1 mM ATP at 20 °C. *C*, the percentage of moving actin filaments in EGTA (*left panel*, *blue bars*) and at *p*Ca 4 (*right panel*, *yellow bars*) as a function of surface myosin density in the presence of 1 mM ATP. The sliding velocity of actin filaments is shown (*black circles*). *D*, the percentage of moving actin filaments in EGTA (*left panel*, *blue bars*) and at *p*Ca 4 (*right panel*, *yellow bars*) as a function of ATP concentration at 240 myosin molecules μm^{-2}. The sliding velocity of actin filaments is shown (*black circles*).

The continuous movement of actin filaments driven by myosin XI was basically recovered by initially washing excess Ca^{2+} out of the flow cell with EGTA-containing buffer and successively adding fresh actin filaments. However, exogenous wild-type CaM (10 μM in EGTA-containing buffer) was required to recover the motility of myosin exposed to Ca^{2+} levels exceeding *p*Ca 5. This result suggests reversible dissociation of CaM at high Ca^{2+} levels (Fig. 1*B*).

The dissociation of CaM and the threshold concentration of Ca^{2+} required for the dissociation were confirmed by an immunoprecipitation assay in which CaM was dissociated from myosin XI when the myosin was treated with a solution above *p*Ca 5 (supplemental Fig. 1). This result is consistent with the necessity of exogenous CaM for recovery of motility at *p*Ca 4. Because of the minute signals and nonlinearity of CaM, quantitative analysis was not possible.

Even in the presence of a high concentration of Ca^{2+} (*p*Ca 4), increasing the surface density of myosin to >500 molecules μm^{-2} (Fig. 1*C*) or decreasing the ATP concentration below 10 μM (Fig. 1*D*) revived the continuous sliding movement of actin filaments. Under these conditions, the velocity of myosin XI decreased below one-third of that observed in the presence of 1 mM EGTA (*p*Ca > 8). These results suggest that although its processivity is reduced, myosin XI retains motility even at *p*Ca 4.

Effects of Ca^{2+} on Kinetic Properties of Myosin XI—The steady-state actin-activated ATPase activity at various Ca^{2+} concentrations revealed that fully activated ATPase in the presence of 24 μM F-actin and 1 mM ATP was not significantly influenced by Ca^{2+} concentration (Fig. 2*A*). The K_{app} for F-actin at *p*Ca 4 was 11.0 ± 2.0 μM, which is slightly higher than in the presence of 1 mM EGTA (10.0 ± 1.1 μM) (Fig. 2*B*). Kinetic processivity, defined as the average number of ATPase cycles per diffusion encounter with F-actin, was estimated from k_{cat}/K_{app} (22); it was 7.8×10^6 M^{-1} s^{-1} in the presence of 1 mM EGTA and 6.4×10^6 M^{-1} s^{-1} at *p*Ca 4. To assess kinetic processivity, k_{cat}/K_{app} should be directly compared with the rate constant (k_{on}) of myosin binding to actin filaments. However, assuming that k_{on} in the presence of 1 mM EGTA is the same as that at *p*Ca 4, the estimated k_{cat}/K_{app} suggests that myosin XI retains kinetic processivity even at high Ca^{2+} concentrations.

Electron Microscopic Observations—Changes in molecular morphology coupled with the dissociation of CaM were examined by electron microscopy. Negatively stained myosin XI molecules observed under an electron microscope showed that many myosin molecules exposed to *p*Ca 4 had relatively short neck domains (Fig. 3*A*). This suggests that the single α-helix of an exposed CaM-binding site becomes disorganized into random coils via hydrophobic or electrostatic interactions. Furthermore, the cord length becomes shorter than a single α-helix. To measure the length of the neck domain, we examined all myosin images with sufficient contrast regardless of the length of the neck domain; we also measured the length from the base of the neck to the tip of the head because it is difficult to distinguish the head and neck domains and to determine the precise location of the head-neck junction. The length from the base of
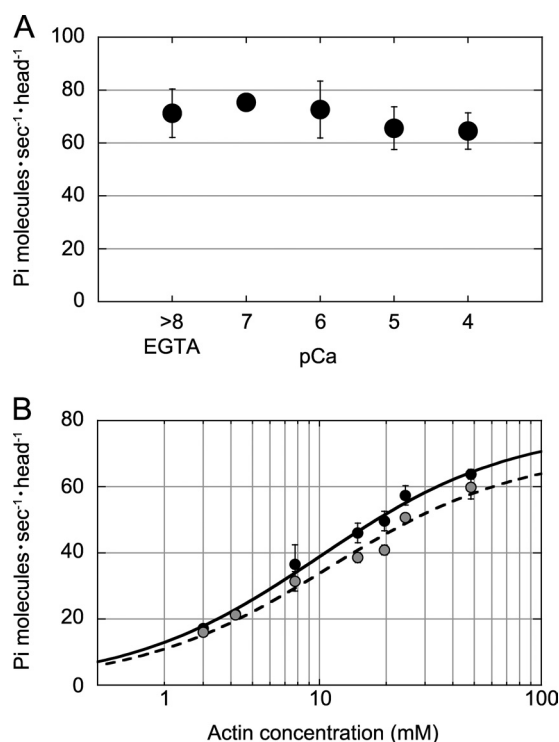
FIGURE 2. **Effects of Ca²⁺ on ATPase activity of myosin XI.** *A*, actin-activated ATPase activity in the presence of 24 μM F-actin and 1 mM ATP at various Ca²⁺ concentrations. *B*, dependence of the actin-activated ATPase rate upon F-actin concentration in the presence of 1 mM ATP in EGTA (*black circles*) and at *p*Ca 4 (*gray circles*). The curves are Michaelis-Menten-fitted. The maximum rate in the presence of 1 mM EGTA was $V_{max} = 77.7 \pm 3.1$ s⁻¹ head⁻¹ and $K_{app} = 10.0 \pm 1.1$ μM, and that at *p*Ca 4 was $V_{max} = 70.9 \pm 4.8$ s⁻¹ head⁻¹ and $K_{app} = 11.0 \pm 2.0$ μM. All measurements were performed in the assay buffer used for the *in vitro* motility assay in the presence of 1 mM ATP at 20 °C.

the neck to the tip of head of intact myosin XI was 32.8 ± 6.0 nm ($n = 128$), which corroborates a result obtained previously by rotary shadowing (9). In contrast, this length was shortened to 27.1 ± 5.7 nm ($n = 272$) when the myosin was exposed to *p*Ca 4 (Fig. 3*B*). Assuming that the length of a neck domain with six light chains is ~25 nm and the length of each light chain is 4 nm (23), we calculated the length of the head domain of myosin XI to be 9 nm. Judging from these observations, one or two CaM molecules probably dissociated from the neck domain (Fig. 3*C*). This estimation is consistent with observations on myosin V using assays on gels (24) or single-molecule analysis (15).

The CaM-binding site has a consensus sequence known as the IQ motif (IQ*XXX*RG*XXX*R), which is highly basic, hydrophobic, and α-helical in structure (25); it is stabilized by the attachment of CaM (26). It is conceivable that the dissociation of CaMs from IQ motifs exposes a single α-helix composed of hydrophobic peptides and leads to the partial melting and shrinking of the α-helix. In addition, Ca²⁺-saturated CaM binding to IQ sequences can form a 1:1 bridging complex with high affinity (27), which would lead to an irregular shape of the lever arm and reduced stiffness. The shortening of the neck domain concomitant with light chain dissociation has also been reported for scallop myosin II (28).

Optical Trap Nanometry at the Single-molecule Level—To examine changes in the mechanical properties of myosin XI, we performed an *in vitro* motility assay with optical trap nanom-

etry to study the movement of 200-nm diameter beads coated with myosin XI molecules at low stoichiometry (9). Rates of occurrence of movement were examined in each myosin-bound bead sample both in the presence of EGTA and at *p*Ca 4, and we confirmed that the rate was almost the same under both conditions. This consistency excludes the possibility that the measurement picked up only the rare intact myosin (without dissociation of CaM) at *p*Ca 4. The beads were captured by a custom-built optical trap and brought into contact with an actin filament (Fig. 4*A*). When the trap was turned off, the beads started moving. The distances moved by the beads (29) in the presence of Ca²⁺ (*p*Ca 4) and 1 mM ATP were measured (Fig. 4*B*). Beads that moved >700 nm were analyzed because it was difficult to distinguish between displacements <700 nm and Brownian motion when the beads were not captured in the optical trap. A single-exponential fit provided a mean distance traveled of 1.3 ± 0.1 μm, which is similar to the 1.3 ± 0.3 μm measured for intact myosin XI in the presence of 1 mM EGTA and 1 mM ATP (9). Thus, myosin XI still retains processivity even at *p*Ca 4.

To scrutinize processive movement in the presence of Ca²⁺, optical trap nanometry for a single myosin XI molecule was performed. Myosin XI showed processive movement along an actin filament in a stepwise manner, even at *p*Ca 4 (Fig. 4*C*), although the total displacement became shorter than achieved by intact myosin XI. The forces produced by myosin XI were 0.82 ± 0.45 and 0.55 ± 0.29 pN in the presence of EGTA and at *p*Ca 4, respectively. The step size of the myosin in the presence of 1 mM EGTA was almost the same with respect to load, with values of 36.1 ± 0.5 nm under the low-load regime (<0.5 pN) and 35.5 ± 0.4 nm under the high-load regime (0.5–1 pN). In contrast, the step size at *p*Ca 4 decreased as the load on myosin XI increased. The average measured step sizes were 27.5 ± 0.4 nm under the low-load regime (<0.5 pN) and 22.1 ± 0.2 nm under the high-load regime (0.5–1 pN) (Fig. 4*D*). The cutoff force (0.5 pN) was assigned by determining the force level at which 50% of myosin XI molecules detached from the actin filament by reference to the maximum force distribution obtained at *p*Ca 4 (supplemental Fig. 2). Based on the electron microscopic observation in Fig. 3*B*, ~85% of myosin XI molecules at *p*Ca 4 have a shorter neck than intact myosin. Coupled with similar occurrence rates in the presence of Ca²⁺ (*p*Ca 4) and in the absence of Ca²⁺ (EGTA), the probability of bead movement occurring by intact myosin XI at *p*Ca 4 was estimated to be 0.099, meaning that ~90% of these events were measured with myosin XI with a shorter neck at *p*Ca 4. The velocities of beads were measured by fitting lines to segments of movement with between 0 and 0.3 pN in trace both in EGTA and at *p*Ca 4 (9). The velocity observed in EGTA was 6.8 ± 3.3 μm s⁻¹, and that at *p*Ca 4 was 74% of that in EGTA, or 5.1 ± 1.8 μm s⁻¹ (mean $\pm$ S.D., $n = 60$). This value is consistent with the ratio of the lever arm length of myosin observed in solution for EGTA and *p*Ca 4. These results show that the length and rigidity of the neck domain produced by attaching CaM are essential for the generation of large 35-nm steps.
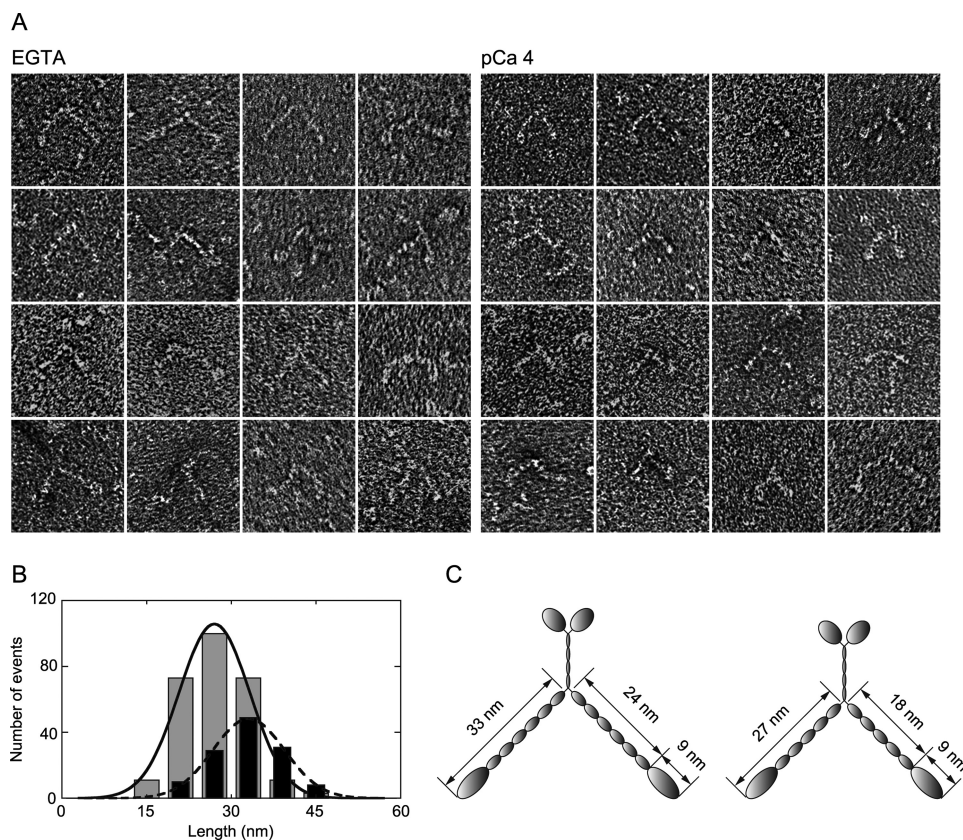
FIGURE 3. **Myosin XI morphology.** *A*, electron micrographs showing morphology of negatively stained myosin XI in EGTA (*left panels*) and at *p*Ca 4 (*right panels*). *B*, lengths from the tip of the head to the base of the neck in EGTA (*black bars*) and at *p*Ca 4 (*gray bars*). The means of fits were 32.8 and 27.1 nm, and the numbers of measurements were 128 and 272, respectively. *C*, illustration of myosin XI before (*left*) and after (*right*) the dissociation of CaMs.

DISCUSSION

To reveal the molecular mechanism of regulation of plant myosin XI is a challenge for understanding how myosin XI works within cells. The parameters measured for myosin XI in EGTA and at *p*Ca 4 are summarized in Table 1. The *in vitro* motility assay revealed that actin filaments were detached from myosin XI concomitant with the reversible detachment of CaM at high Ca^{2+} concentrations. Electron microscopy revealed that the neck length of myosin XI at *p*Ca 4 shortened by 75%, from 24 to 18 nm, suggesting the shrinkage of exposed IQ domains through α-helix destabilization followed by the dissociation of one or two CaM molecules per heavy chain. Optical trap single-molecule analysis revealed that the step size was shortened by 77%, from 35 to 27 nm, under a low-load regime (<0.5 pN), showing a proportional relationship between lever arm length and step size. The 27-nm steps measured are consistent with the ~26-nm steps generated by a myosin Va mutant with four short IQ motifs (12, 30, 31), strongly supporting the shortening of the myosin XI neck followed by the dissociation of one or two CaMs. According to the lever arm model, the strain imposed by the power stroke of a leading head having an intact 24-nm neck domain swings the trailing head 25 nm forward. The trailing head then easily finds the next binding site 35 nm forward on the actin pseudorepeat by performing an 11-nm diffusive search (Fig. 5*A*) (13). In contrast, a myosin Va mutant with four short IQ motifs and its heads spaced about nine actin subunits apart must twist around the actin filament by ~70° (12, 30).

Similarly, at *p*Ca 4, the leading head of myosin XI cannot achieve the same azimuth relative to the actin filament because the short 20-nm neck generates only a short 21-nm power stroke and must twist to attach to the nearest binding site on the actin filament (Fig. 5*B*). Furthermore, the step size decreased to 22.1 ± 0.2 nm under the high-load regime (0.5–1 pN), despite the step size of intact myosin XI being less dependent on load (36.1 ± 0.5 nm under the low load and 35.5 ± 0.4 nm under the high load). This can be explained as follows: the net length able to act as a lever decreases under a high load because of the kink at the IQ motif position where CaM dissociated. According to this hypothesis, the power stroke is defined by the IQ motif position where CaM dissociated. Therefore, the closer the IQ motif position is to the head, the shorter the effective length acting as a lever arm. In the case of myosin Va, a detailed truncation assay revealed that Ca^{2+}-induced CaM dissociation occurs at the second IQ domain (32, 33). The second IQ motif of myosin Va has a sequence that diverges further from the consensus sequence of the IQ motif. In tobacco 175-kDa myosin XI, the fourth IQ motif shows a divergent sequence. If this sequence diversity reflects the IQ motif position where CaM dissociates, the three IQ motifs from the first to the third (12 nm in length) act as an effective lever arm, generating the power stroke, estimated to be 13 nm (Fig. 5*C*). However, the relationship between sequence similarity of the IQ motif and CaM dissociation still remains unclear; our data are reasonable, assuming that CaM dissociates from the fourth IQ motif of myosin XI.
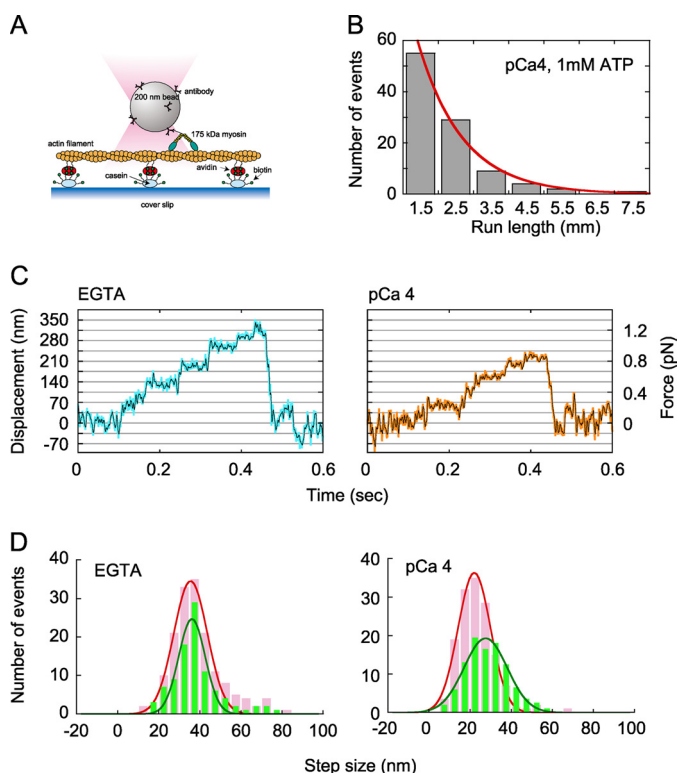
FIGURE 4. **Single-molecule analysis.** *A*, schematic of the experimental arrangement. Partially biotinylated actin filaments (biotinylated actin/non-biotinylated actin = 1:100) were attached to biotinylated casein-coated glass surfaces via avidin. *B*, run length measured after trapping off. *C*, force and movement generated by myosin XI on an actin filament in EGTA (*left panel*) and at *p*Ca 4 (*right panel*) at 1 mM ATP. *Blue* and *orange lines*, raw data; *black lines*, same data passed though a low-pass filter of 100-Hz bandwidth. *D*, step size distribution under low-load (<0.5 pN; *green bars*) and high-load (0.5–1 pN; *pink bars*) regimes. The curve is a normal distribution fitted to the data with peaks at 36.1 ± 0.5 nm (<0.5 pN) and 35.5 ± 0.4 nm (0.5–1 pN) in EGTA and 27.5 ± 0.4 nm (<0.5 pN) and 22.1 ± 0.2 nm (0.5–1 pN) at *p*Ca 4.

TABLE 1

Parameters measured in EGTA and *p*Ca 4

	EGTA	*p*Ca 4
Biochemical data		
V_{max} of ATPase (P_i molecules s^{-1} head^{-1})	77.7 ± 3.1	70.9 ± 4.9
K_m for ATPase (μM)	10.0 ± 1.1	11.0 ± 2.1
k_{cat}/K_{app} (M^{-1} s^{-1})	7.8 × 10^6	6.4 × 10^6
Molecular configuration (EM)		
Length from neck base to head tip (nm)	32.8 ± 6.0	27.1 ± 5.7
***In vitro* assay (ensemble, 960 myosin molecules μm^{-2})**		
$V_{max(e)}$ (μm s^{-1})	4.3 ± 0.7	1.5 ± 0.8
Bead assay (single molecule)		
$V_{max(s)}$ (μm s^{-1})	6.8 ± 3.3	5.1 ± 1.8
Run length at 1 mM ATP (μm)	1.3 ± 0.3[a]	1.3 ± 0.1
Step size (nm)		
Low load (<0.5 pN)	36.1 ± 0.5	27.5 ± 0.4
High load (0.5–1 pN)	35.5 ± 0.4	22.1 ± 0.2
Force (pN)	0.82 ± 0.45	0.55 ± 0.29

[a] Determined in a previous study (9).

Processivity and Velocity Are Lower in an in Vitro Motility Assay Compared with Single-molecule Analysis—The number of steps that a single myosin XI travels on an actin filament without an optical trap was calculated as run length divided by step size; at low load, this was 1.3 μm/28 nm = 46.4 steps at *p*Ca 4. Although this value is an overestimate because run length was measured without load, whereas step size was measured

under load (<0.5 pN), it still suggests that myosin XI at *p*Ca 4 retains sufficient processivity.

We found that processivity and velocity determined in the *in vitro* surface (ensemble) assay are different from those determined in the single-molecule assay. Although intact myosin XI can move actin continuously even at 50 molecules μm^{-2} in the surface assay (9), at *p*Ca 4, almost all actin filaments detached from the surface at a density of 240 myosin molecules μm^{-2}, as if the myosin act as a non-processive motor. On the other hand, single myosin molecules on a bead retain processivity even at *p*Ca 4, as described above. In addition, the velocity at *p*Ca 4 was 35% of that in EGTA in the surface ensemble assay and 74% in the single-molecule assay. These differences can be explained by considering the difference in geometry between the two assays. In an *in vitro* motility assay, the three-dimensional diffusion of the myosin molecule is sterically restricted, particularly with respect to the *z* axis. Therefore, a leading head with a short 20-nm neck cannot search for and bind a proximal actin subunit at a different azimuth because of inflexibility along the *z* axis (Fig. 5*D*). In contrast, a myosin molecule on a bead is able to search and binds the next binding site, about seven to nine actin subunits forward, by twisting. Thus, bead-bound myosin XI is able to achieve multiple steps by searching for the binding site on the upper side of an actin filament, which is fixed on the surface without revolving around the filament (Fig. 5, *B* and *C*). The difference in velocity determined in ensemble and single-molecule assays can be explained by considering the effective power stroke. In the surface ensemble assay, individual myosin molecules would work under an internal load. Because a kink occurs at the fourth IQ motif under an internal load, the effective power stroke will be 13 nm, generated by a 12-nm lever arm. Furthermore, both the kink and inflexibility along the *z* axis inhibit binding of the leading head to the next binding site with a different azimuth. As a result, myosin XI behaves as if it is a single-headed motor with a short 12-nm lever arm, generating a 13-nm power stroke, which is 37% of a 35-nm step (Fig. 5*D*). Although this model is speculative and needs further study, it explains the differences in results between ensemble surface and single-molecule assays.

Comparison of the Molecular Mechanism for Ca^{2+} Regulation of Myosin V—Recently, several studies revealed that Ca^{2+} can affect myosin V motility in at least two ways. Full-length myosin V adopts a folded inhibited conformation in EGTA when cargo is not present (34–37). At low Ca^{2+} concentrations or when cargo binds in the absence of Ca^{2+}, myosin V becomes unfolded and active. Higher Ca^{2+} concentrations inhibit processive movement via the dissociation of one or two CaM molecules (14, 15, 34, 36). In our study using tissue-purified full-length tobacco 175-kDa myosin XI, neither the folded conformation nor inactivation of ATPase activity in EGTA was detected, indicating that head-to-tail interaction is not equipped for this regulatory mechanism. Tobacco 175-kDa myosin XI can be regulated by Ca^{2+} in one way, through the reversible dissociation of CaM. The situation is the same as that for myosin V heavy meromyosin (a globular tail domain-truncated dimeric construct), which cannot adopt a folded conformation. At the single-molecule level, free myosin V heavy meromyosin shows no processive movement on immobilized actin
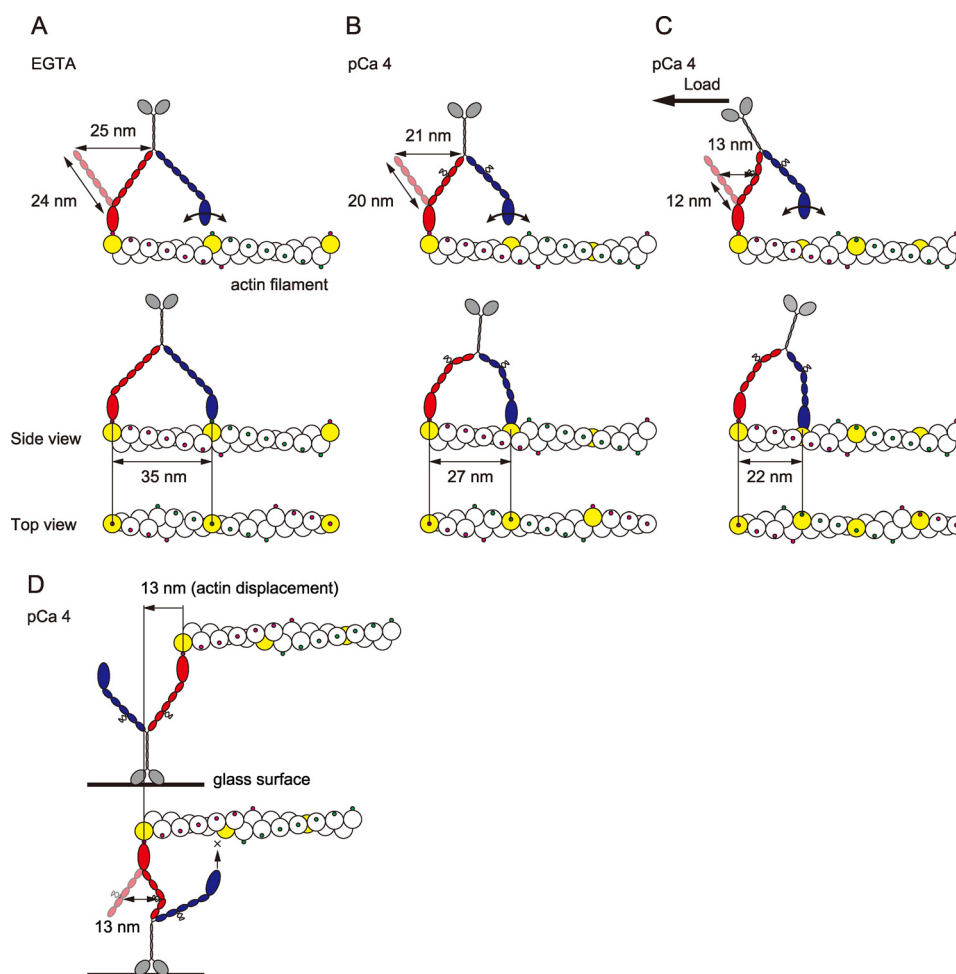
FIGURE 5. **Model of the stepwise movement of myosin XI after Ca^{2+}-induced CaM dissociation along an actin filament.** In each case, the lead head is colored *red*, and the trail head is *blue*. The putative actin subunit for binding estimated from step size is colored *yellow*. *A*, in EGTA, myosin XI generates 35-nm steps along the same azimuth on an actin filament with a long 27-nm neck. *B*, at *p*Ca 4, the leading head cannot achieve the same azimuth relative to the actin filament because it has a short neck with four to five light chains, generating 27-nm steps, landing at a different azimuth about nine actin subunits forward. *C*, under the high load, the kink at the position in the fourth IQ motif due to the load causes the lever to act as if it has three light chains, generating 22-nm steps, landing about seven actin subunits forward. Myosin XI is able to achieve multiple steps, searching and then binding to the binding site at the upper side of the actin filament. *D*, in an *in vitro* motility assay, the diffusion of myosin is sterically restricted, especially on the *z* axis, which inhibits processive movement. The actin displacement is 13 nm, which is 37% of the 35 nm generated by intact myosin XI.

filaments in the presence of Ca^{2+} without extra CaM (14). In one report, the V_{max} of actin-activated ATPase activity at high Ca^{2+} in the absence of CaM was markedly decreased (24), whereas in another, V_{max} was slightly increased, but the K_m for actin was not affected (34). In our study, high Ca^{2+} concentration slightly affected both mechanical (run length) and kinetic processivity. What causes the differential sensitivity to Ca^{2+} with respect to processive movement between myosins V and XI? We speculate that even at the same Ca^{2+} concentration, processivity can be altered depending on the IQ motif position where CaM dissociates, proximal or distal to the motor domain. For example, CaM dissociation from the second IQ motif (in myosin Va) may induce a more drastic reduction of processivity than from the fourth IQ motif (in tobacco 175-kDa myosin XI) because the effective neck length acting as a lever arm is 4 nm in myosin Va and 12 nm in myosin XI. Our study suggests that the change in motile properties under varying Ca^{2+} conditions is caused mainly by a mechanical change to the neck domain through reversible dissociation of CaM. However, the possibility remains that Ca^{2+} affects the kinetic properties of the motor

domain, such as the duty ratio (38, 39). Elucidation of these possibilities awaits additional detailed kinetic studies.

Implications for the Regulation of Cytoplasmic Streaming in Plant Cells—Cytoplasmic streaming has been considered to be generated by the movement of myosin-coated organelles along relatively static actin bundles fixed inside the cell. This situation is similar to the bead assay, in which myosin moves along an actin filament fixed on the glass surface. However, it has been suggested that tobacco 175-kDa myosin XI is a molecular motor responsible for translocation of the endoplasmic reticulum in tobacco BY-2 cells (17, 40). Furthermore, recent studies reported that a deficiency in myosin XI affects the orientation of the actin filament bundles (41, 42). To explain this phenomenon, a three-way interaction model was proposed. The directional arrangement of actin bundles requires the interaction and strain between the bundle and the large membranous organelle via myosin. In this model, myosin XI molecules bridging the gap between a large organelle and the actin cable might be under loaded conditions and stretched. This situation is similar to the *in vitro* motility assay rather than the bead assay. In

contrast, myosin Va is responsible for relatively small organelle or vesicle transport (43). Our results suggest that Ca^{2+}-induced CaM dissociation would act as a load-dependent regulator for myosin processivity and that the IQ motif position of CaM dissociation is optimized for myosin-specific organelle transport *in vivo*.

REFERENCES

1. Kamiya, N. (1981) Physical and chemical basis of cytoplasmic streaming. *Annu. Rev. Plant Physiol.* **32,** 205–236
2. Shimmen, T., and Yokota, E. (1994) Physiological and biochemical aspects of cytoplasmic streaming. *Int. Rev. Cytol.* **155,** 97–139
3. Shimmen, T. (2007) The sliding theory of cytoplasmic streaming: fifty years of progress. *J. Plant Res.* **120,** 31–43
4. Reddy, A. S. (2001) Molecular motors and their functions in plants. *Int. Rev. Cytol.* **204,** 97–178
5. Kohno, T., and Shimmen, T. (1988) Accelerated sliding of pollen tube organelles along Characeae actin bundles regulated by Ca^{2+}. *J. Cell Biol.* **106,** 1539–1543
6. Doree, M., and Picard, A. (1980) Release of Ca^{2+} from intracellular pools stops cytoplasmic streaming in *Tradescantia* staminal hairs. *Experientia* **36,** 1291–1292
7. Woods, C. M., Polito, V. S., and Reid, M. S. (1984) Response to chilling stress in plant cells. II. Redistribution of intracellular calcium. *Protoplasma* **121,** 17–24
8. Takagi, S., and Nagai, R. (1986) Intracellular Ca^{2+} concentration and cytoplasmic streaming in *Vallisneria* mesophyll cells. *Plant Cell Physiol.* **27,** 953–959
9. Tominaga, M., Kojima, H., Yokota, E., Orii, H., Nakamori, R., Katayama, E., Anson, M., Shimmen, T., and Oiwa, K. (2003) Higher plant myosin XI moves processively on actin with 35-nm steps at high velocity. *EMBO J.* **22,** 1263–1272
10. Yokota, E., Muto, S., and Shimmen, T. (1999) Inhibitory regulation of higher plant myosin by Ca^{2+} ions. *Plant Physiol.* **119,** 231–240
11. Moore, J. R., Krementsova, E. B., Trybus, K. M., and Warshaw, D. M. (2001) Myosin V exhibits a high duty cycle and large unitary displacement. *J. Cell Biol.* **155,** 625–635
12. Purcell, T. J., Morris, C., Spudich, J. A., and Sweeney, H. L. (2002) Role of the lever arm in the processive stepping of myosin V. *Proc. Natl. Acad. Sci. U.S.A.* **99,** 14159–14164
13. Veigel, C., Wang, F., Bartoo, M. L., Sellers, J. R., and Molloy, J. E. (2002) The gated gait of the processive molecular motor, myosin V. *Nat. Cell Biol.* **4,** 59–65
14. Lu, H., Krementsova, E. B., and Trybus, K. M. (2006) Regulation of myosin V processivity by calcium at the single molecule level. *J. Biol. Chem.* **281,** 31987–31994
15. Nguyen, H., and Higuchi, H. (2005) Motility of myosin V regulated by the dissociation of single calmodulin. *Nat. Struct. Mol. Biol.* **12,** 127–132
16. Walker, M. L., Burgess, S. A., Sellers, J. R., Wang, F., Hammer, J. A., 3rd, Trinick, J., and Knight, P. J. (2000) Two-headed binding of a processive myosin to F-actin. *Nature* **405,** 804–807
17. Yokota, E., Ueda, S., Tamura, K., Orii, H., Uchi, S., Sonobe, S., Hara-Nishimura, I., and Shimmen, T. (2009) An isoform of myosin XI is responsible for the translocation of endoplasmic reticulum in tobacco cultured BY-2 cells. *J. Exp. Bot.* **60,** 197–212
18. Yokota, E., Yukawa, C., Muto, S., Sonobe, S., and Shimmen, T. (1999) Biochemical and immunocytochemical characterization of two types of myosins in cultured tobacco bright yellow-2 cells *Plant Physiol.* **121,** 525–534
19. Muto, S., and Miyachi, S. (1984) Production of antibody against spinach calmodulin and its application to radioimmunoassay for plant calmodulin. *Z. Pflanzenphysiol.* **114,** 421–431
20. Nishiyama, M., Muto, E., Inoue, Y., Yanagida, T., and Higuchi, H. (2001) Substeps within the 8-nm step of the ATPase cycle of single kinesin molecules. *Nat. Cell Biol.* **3,** 425–428
21. Kron, S. J., Toyoshima, Y. Y., Uyeda, T. Q., and Spudich, J. A. (1991) Assays for actin sliding movement over myosin-coated surfaces. *Methods Enzymol.* **196,** 399–416
22. Hackney, D. D. (1995) Highly processive microtubule-stimulated ATP hydrolysis by dimeric kinesin head domains. *Nature* **377,** 448–450
23. Howard, J. (1997) Molecular motors: structural adaptations to cellular functions. *Nature* **389,** 561–567
24. Homma, K., Saito, J., Ikebe, R., and Ikebe, M. (2000) Ca^{2+}-dependent regulation of the motor activity of myosin V. *J. Biol. Chem.* **275,** 34766–34771
25. Wolenski, J. S. (1995) Regulation of calmodulin-binding myosins. *Trends Cell Biol.* **5,** 310–316
26. Bähler, M., and Rhoads, A. (2002) Calmodulin signaling via the IQ motif. *FEBS Lett.* **513,** 107–113
27. Martin, S. R., and Bayley, P. M. (2004) Calmodulin bridging of IQ motifs in myosin V. *FEBS Lett.* **567,** 166–170
28. Flicker, P. F., Wallimann, T., and Vibert, P. (1983) Electron microscopy of scallop myosin. Location of regulatory light chains. *J. Mol. Biol.* **169,** 723–741
29. Howard, J. (2001) *Mechanics of Motor Proteins and the Cytoskeleton*, Sinauer Associates, Sunderland, MA
30. Sakamoto, T., Yildez, A., Selvin, P. R., and Sellers, J. R. (2005) Step size is determined by neck length in myosin V. *Biochemistry* **44,** 16203–16210
31. Oke, O. A., Burgess, S. A., Forgacs, E., Knight, P. J., Sakamoto, T., Sellers, J. R., White, H., and Trinick, J. (2010) Influence of lever structure on myosin 5a walking. *Proc. Natl. Acad. Sci. U.S.A.* **107,** 2509–2514
32. Koide, H., Kinoshita, T., Tanaka, Y., Tanaka, S., Nagura, N., Meyer zu Hörste, G., Miyagi, A., and Ando, T. (2006) Identification of the single specific IQ motif of myosin V from which calmodulin dissociates in the presence of Ca^{2+}. *Biochemistry* **45,** 11598–11604
33. Trybus, K. M., Gushchin, M. I., Lui, H., Hazelwood, L., Krementsova, E. B., Volkmann, N., and Hanein, D. (2007) Effect of calcium on calmodulin bound to the IQ motifs of myosin V. *J. Biol. Chem.* **282,** 23316–23325
34. Krementsov, D. N., Krementsova, E. B., and Trybus, K. M. (2004) Myosin V: regulation by calcium, calmodulin, and the tail domain. *J. Cell Biol.* **164,** 877–886
35. Wang, F., Thirumurugan, K., Stafford, W. F., Hammer, J. A., 3rd, Knight, P. J., and Sellers, J. R. (2004) Regulated conformation of myosin V. *J. Biol. Chem.* **279,** 2333–2336
36. Li, X. D., Mabuchi, K., Ikebe, R., and Ikebe, M. (2004) Ca^{2+}-induced activation of ATPase activity of myosin Va is accompanied with a large conformational change. *Biochem. Biophys. Res. Commun.* **315,** 538–545
37. Liu, J., Taylor, D. W., Krementsova, E. B., Trybus, K. M., and Taylor, K. A. (2006) Three-dimensional structure of the myosin V inhibited state by cryo-electron tomography. *Nature* **442,** 208–211
38. Liao, W., Elfrink, K., and Bähler, M. (2010) Head of myosin IX binds calmodulin and moves processively toward the plus-end of actin filaments. *J. Biol. Chem.* **285,** 24933–24942
39. Stöffler, H. E., and Bähler, M. (1998) The ATPase activity of Myr3, a rat myosin I, is allosterically inhibited by its own tail domain and by Ca2+ binding to its light chain calmodulin. *J. Biol. Chem.* **273,** 14605–14611
40. Yokota, E., Ueda, H., Hashimoto, K., Orii, H., Shimada, T., Hara-Nishimura, I., and Shimmen, T. (2011) Myosin XI-dependent formation of tubular structures from endoplasmic reticulum isolated from tobacco cultured BY-2 cells. *Plant Physiol.* **156,** 129–143
41. Ueda, H., Yokota, E., Kutsuna, N., Shimada, T., Tamura, K., Shimmen, T., Hasezawa, S., Dolja, V. V., and Hara-Nishimura, I. (2010) Myosin-dependent endoplasmic reticulum motility and F-actin organization in plant cells. *Proc. Natl. Acad. Sci. U.S.A.* **107,** 6894–6899
42. Peremyslov, V. V., Prokhnevsky, A. I., and Dolja, V. V. (2010) Class XI myosins are required for development, cell expansion, and F-actin organization in *Arabidopsis*. *Plant Cell* **22,** 1883–1897
43. Desnos, C., Huet, S., and Darchen, F. (2007) "Should I stay or should I go?": myosin V function in organelle trafficking. *Biol. Cell* **99,** 411–423